PCCP

PAPER

View Article Online
View Journal | View Issue

Cite this: *Phys. Chem. Chem. Phys.*, 2022, **24**, 2646

Electronic structures of the MoS_2/TiO_2 (anatase) heterojunction: influence of physical and chemical modifications at the 2D- or 1D-interfaces†

Rémi Favre, [a] Pascal Raybaud *[ab] and Tangui Le Bahers *[a]

To tackle the challenge of CO_2 photoreduction, semiconducting layered transition metal dichalcogenides like MoS_2 have attracted much attention due to their tunable 2D nano-structures. By using advanced periodic density functional theory calculations (HSE06 functional), we provide a systematic quantification of the optoelectronic properties of various interfacial heterostructures composed of 2H-MoS_2 and anatase TiO_2. We systematically determine the band gaps, and conduction band (CB) and valence band (VB) positions to figure out the nature of the heterojunction. Two main surface orientations of anatase TiO_2 particles, (101) and (001), are considered with 2D-MoS_2 nanosheets or nanoribbons forming either a 2D physical (van der Waals) or through a 1D chemical interface. The possibility to chemically modify the MoS_2/TiO_2 interface, either by sulfidation or hydration, and its effect on the electronic structure are deeply investigated. These modifications in the heterostructure lead to important changes in the electronic properties and charge transfer between the two materials which impact both photon absorption properties and charge carrier dynamics suspected to influence in turn the photocatalytic activity. While a type I hetrojunction is found for the 1D chemical interface, a type II heterojunction with appropriate CB/VB positions for CO_2 reduction and H_2O oxidation is identified for the 2D physical interface which could lead to the targeted Z-scheme mechanism with strong potential interest in photocatalysis applications.

Received 10th November 2021,
Accepted 4th January 2022

DOI: 10.1039/d1cp05151b

rsc.li/pccp

Introduction

Motivated by the fruitful progress of the research on photocatalytic water splitting to produce H_2,[1–3] the strong interest in CO_2 photoreduction into solar fuels is growing within the community of heterogeneous photocatalysis[4,5] for economic and ecological interests. Unfortunately, this topic appears to be much more challenging for several reasons. Carbon dioxide is involved in many oxidation–reduction couples and could be reduced to different valuable products (CH_4, CH_3OH, HCOOH, CO...) prompting the control of the selectivity depending on the targeted process. Moreover, these reactions involve a high number of electrons (up to 8). Last but not least, the CO_2 reduction mechanism is still unclear and could require a large electrochemical potential to perform the first electron transfer. All of this leads to the actual systems with an energy conversion efficiency around 1%,[6] far from the targeted value of 10%.[7]

In order to tackle the challenging development of photocatalytic CO_2 reduction, numerous studies are exploring various classes of promising semiconducting materials that could offer new perspectives in the photocatalysis research. Among these materials, transition metal dichalcogenides, such as 2H-MoS_2, are attracting attention for their stability (against air, oxygen and sulfur) and their optoelectronic properties adapted for photocatalysis, as highlighted by several experimental works.[8,9] Moreover, this 2D-MoS_2 material presents a nano-structure that could be easily tuned (doping elements, number of layers, size of the nanosheet...) in order to adapt its optoelectronic properties as a function of the requirements.[10] However, the limitation of the use of MoS_2 in photocatalysis may raise from its slightly too small bandgap (between 1.3[11] and 1.9[12] eV as a function of the number of layers). As an example, to realize efficiently the photoreduction of CO_2 in HCOOH at pH = 0 with H_2O as the reducer, a bandgap higher than 2.1 eV would be necessary with properly tuned positions of the conduction and valence bands (CB/VB).[5]

[a] *Univ Lyon, ENS de Lyon, CNRS, Université Claude Bernard Lyon 1, Laboratoire de Chimie UMR 5182, F-69342, France. E-mail: pascal.raybaud@ifpen.fr, tangui.le_bahers@ens-lyon.fr*

[b] *IFP Energies Nouvelles, Rond-point de l'échangeur de Solaize, BP 3, 69360 Solaize, France*

† Electronic supplementary information (ESI) available. See DOI: 10.1039/d1cp05151b

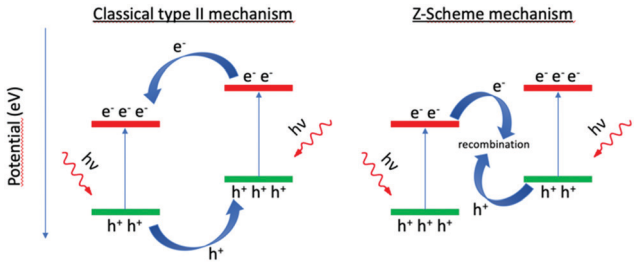

Fig. 1 Comparison of the classical type II mechanism and the Z-scheme mechanism.

To overcome this challenge, the possibility of a Z-scheme mechanism[13,14] based on the interaction of MoS_2 with another well-chosen semiconductor is often explored. This specific mechanism could be made possible by the use of type II heterojunction (Fig. 1), where the absorption of two photons is followed by an electron–hole recombination at the interface between the two semiconductors. In a Z-scheme working principle, the interface built between two small bandgap materials, allows to reach highly reactive and spatially separated charge carriers. The choice of the second semiconductor is thus driving not only the band gap itself but also by the relative positions of the conduction and valence bands (CB/VB). The orientation towards a classical type II mechanism or a Z-scheme depends on various factors such as band bending, interfacial electric field or the dynamics of charge transfer which are challenging parameters to control.[13,14]

Due to the low-cost, high stability and abundance of the 2H-MoS_2 and anatase-TiO_2 materials, MoS_2/TiO_2 heterostructure has been the subject of numerous studies[15,16] combining the efficient photocatalytic properties of TiO_2[17,18] with the well-known catalytic activity of MoS_2 for the activation, conversion and production of various molecules.[19,20] MoS_2 may act as a cocatalyst with the aim to harvest the photogenerated charges in order to avoid the recombination of the electrons and holes photogenerated in TiO_2. The charge carriers collected and the active sites of MoS_2 offers a large range of applications (degradation of organic pollutants,[21,22] CO_2 reduction,[23] Hydrogen Evolution Reaction[24]...). In general, investigations on MoS_2/TiO_2 nano composites are focusing on the Hydrogen Evolution Reaction. Efficient nano composites are composed of MoS_2 nanosheets coated on TiO_2 in a core–shell structure. The TiO_2 core could have different shapes (nanowire,[25] nanobelt[26] or nanotubes[27]). Since the (101) surface is known to be the most stable and the predominant surface,[28,29] it is generally proposed that the MoS_2 layers are mainly located on this surface. However, a recent study focusing on a 2D MoS_2 monolayer deposited on the (001) surface of anatase TiO_2 nanosheet,[30] revealed that photocatalytic activity in H_2 evolution from water is 36.4 times higher than on pure TiO_2 nanosheet and even 2 times higher than Pt/TiO_2, showing the high potential interest of MoS_2/TiO_2 as photocatalytic system. However, despite the strategies considered to increase the HER performance (MoS_2 engineering, interface engineering, use of photosensitizer or sacrificial agent), the best photoactivities obtained (16.7 mmol g^{-1} h^{-1} [25] and 2.2 mmol g^{-1} h^{-1} [22]) are still not satisfying. From the CO_2 photoreduction point of view, the few results obtained with MoS_2/TiO_2 nanosheets are promising with an activity of 10.6 μmol g^{-1} h^{-1}, 3 times higher than pure TiO_2 nanosheets and 2 times higher than Pt/TiO_2 0.5 wt% Pt.[23]

As presented above, the photoactivity obtained with the MoS_2/TiO_2 heterostructure is particularly appealing but remains to be improved for several reasons. First, the mismatch between MoS_2 and TiO_2 lattice leads to a highly defective interface with only a small amount of MoS_2 in direct contact with TiO_2. Second, MoS_2/TiO_2 architectures are facing the limitations of poor visible-light harvesting, low electrical conductivity and deficient catalytic active sites prompting the deeper optimization of the nano-structuration to overcome these drawbacks. In particular, the impact of the structure of the MoS_2/TiO_2 heterojunction (nature of the TiO_2 crystallographic facets, chemical or physical interaction between MoS_2 and TiO_2, chemical composition of the interface) on the optoelectronic properties is not known. Hence, providing a detailed atomistic description of the MoS_2/TiO_2 interface will undoubtedly open perspectives on this heterostructure design for photocatalytic applications.

With the aim at providing rational guides for the materials' nanostructuration of the TiO_2/MoS_2 interface, we propose in the present work to explore the evolution of the band gap and conduction band (CB)/valence band (VB) positions of various 1D- or 2D-MoS_2/TiO_2-anatase heterojunctions by using state of the art periodic density functional theory (DFT) calculations. We will focus on the two main surface orientations of anatase TiO_2 particles ((101) and (001)). The contribution of the (001) surface orientation, neglected for its minor presence on anatase particles in vacuum conditions,[28] could become more predominant under aqueous environment[29] encountered in reactions involving water as a reactant (such as water splitting). Hence, it will be also considered carefully in this work. In addition, beyond the physical van der Waals interaction (2D), the chemical epitaxy-like interaction (1D) which has been reported in the literature[31–33] will be also investigated. Moreover, the influence of key physico-chemical parameters of the interface on the CB/VB positions will be studied: sulfidation and hydration states, orientation of the MoS_2 nano-sheets, size of MoS_2 nano-ribbons.

The objective of this study is thus to provide a general view on the evolution of the band positions and the possible charge carrier pathways after the heterojunction as a function of physico-chemical parameters accessible experimentally. The feasibility of a Z-scheme mechanism, different from the classical type II mechanism will also be discussed.

Methods

DFT calculations were all performed using Vienna *Ab Initio* Simulation Package (VASP) code.[34,35] Geometry optimizations were performed using the PBE functional,[36] followed by a single

point calculation using the range separated hybrid HSE06 functional[37] along with a cut off-energy of 500 eV. In both cases, the van der Waals contributions were described using the Grimme D3 approach with Becke–Johnson damping (D3-BJ).[38] The precision setting of VASP was set to ''Normal'' and a Gaussian smearing 0.05 eV was used. The convergence criterion for the SCF cycle was fixed at 10^{-7} eV per unit cell and the maximum forces were converged to below 0.02 eV $Å^{-1}$ during the geometry optimization. Complementary spin polarized calculations were performed when necessary (Supporting Information 5, ESI†).

To mimic aqueous conditions, in which water could be used either as a reactant or could be produced by the redox reactions, implicit water solvent was added in interfacial systems and independent ones using the VASPsol code.[39]

The TiO_2 anatase (101) and the (001) surfaces were considered (Fig. S1, ESI†). For the (001) surface, in addition to implicit water solvation (as described before), explicit hydration of the surface was used with a water coverage of 3.5 H_2O per nm^2 was considered because it was shown that in ambient conditions hydroxyl groups stabilize the Ti sites present on the bare surface.[29] This effect on electronic properties has been tested as reported in the result section. A 12 × 12 × 1 *k*-point mesh was used for the calculations on the separated materials (TiO_2 surfaces and MoS_2 monolayer). A vacuum thickness of 20 Å was used based on convergence calculations (Supporting Information 8, ESI†).

For the physical interaction, one infinite 2D-MoS_2 nanosheet has been chosen which is known to exhibit larger bandgap than multilayers.[10] For the heterojunction, the MoS_2 nanosheet was optimized in parallel orientation with respect to the TiO_2 surfaces leading to a 2D-interface. For that, the unit cell of the two materials was multiplied in order to respect the commensurability of the respective lattice parameters (Fig. S2, ESI†).

In the case of MoS_2 on TiO_2 anatase (101), we used a 5 × 2 × 1 supercell for MoS_2 on a 4 × 1 × 1 supercell for TiO_2 with a MoS_2 dilatation of 2.12% on the x axis and 4.26% on the y axis. On the (001) surface, we used a 5 × 3 × 1 supercell for MoS_2 on a 4 × 4 × 1 supercell for TiO_2 with a MoS_2 dilatation of 2.57% on the x axis and 6.60% on the y axis. Based on convergence calculations presented in Supporting Information 8 (ESI†), a reduced *k*-point mesh was used: 4 × 4 × 1 for the geometry optimizations at PBE-D3 level and 1 × 1 × 1 for the single point HSE06 calculations. Valence and conduction bands are determined from the last occupied state and the first unoccupied one. The Fermi level corresponds to the top of the valence band. These values are then adjusted with respect to the vacuum potential, different for each calculation, and determined by plotting the local electrostatic potential (Fig. S3, ESI†).

For the chemical interaction, we chose one finite size MoS_2 nanoribbon exposing edges forming Mo–O–Ti or Mo–S–Ti chemical bonding along a 1D-interface with TiO_2. A tilting angle of the nanoribbon with respect to the TiO_2 surface is observed after geometry optimization. Various sizes of the nano-ribbon have been simulated. More details will be given in the results section.

In order to avoid artificial dipole moment in slab structures, symmetric slabs were modelled with one MoS_2 nanosheet added on each side of the TiO_2 slab leading to systems containing between ~300 and ~500 atoms.

We determined the electronic adhesion energies of each system. This energy descriptor aims at apprehending the relevancy and realism of the proposed systems at first order. Due to the size of systems, an exhaustive study of absolute thermodynamic stability as a function of conditions which would include vibrational analysis is beyond the scope of this study.

Results

MoS_2 2D-monolayer in physical interaction with TiO_2 anatase surfaces

Bare and hydrated TiO_2 surfaces. Before investigating the heterostructures, the influence of explicit hydration of TiO_2 surfaces on their electronic structure revealed that while the electronic structure of the (101) surface is weakly affected by water molecules, the presence of an explicit solvation by adding dissociated water on the Ti and O sites of the (001) surface has a large impact on the bandgap and VB/CB positions, which is mandatory to recover the experimental values (Fig. S8, ESI†). A similar impact of dissociated water on rutile and anatase surfaces was reported by a previous theoretical study.[40] As a matter of fact, a 3.5 H_2O per nm^2 coverage (*i.e.* 8 water molecules by unit cell adsorbed in a dissociative way) is required to reach the 3.3 eV bandgap expected for TiO_2 anatase surfaces. The (001) surface with hydration of 3.5 H_2O per nm^2 corresponds to the presence of one hydroxyl (OH) group per surface Ti atom, without residual molecular water.[29] By contrast, the (101) surface was shown to stabilize non-dissociated water, with almost no influence on the bandgap. As a consequence, in what follows the bare (101) surface was modeled only while the (001) one was explicitly solvated.

As a starting point for the investigation of the TiO_2/MoS_2 heterostructures, we focused on structures with MoS_2 physically adsorbed on TiO_2, *i.e.* interacting by van der Waals forces and eventually also by hydrogen bonding with TiO_2 (Fig. 2). For these architectures, the weak interaction energies (−0.21 eV per MoS_2 for (101) and −0.10 eV per MoS_2 for (001)) and the large average distances between the O plane (of the surface for (101) and of the hydroxyls for (001)) and the S plane (2.87 Å for (101) and 3.02 Å for (001)) supports the idea of a van der Waals type of interaction, as reported in the literature for similar systems.[25,26,41]

As a consequence of these weak interactions between TiO_2 and MoS_2 in van der Waals heterostructures, the electronic structures of the interface can be seen as the sum of the electronic structures of the two individual materials (Fig. 2). The interface is a Type-II heterostructure (Fig. 1) characterized by the existence of a bandgap (1.26 eV for (101) and 1.45 eV for (001)), with a valence band located on MoS_2 and a conduction band located on TiO_2.

The density of states (DOS) with the projected states on each element (Fig. S9, ESI†), show that the valence band is mainly

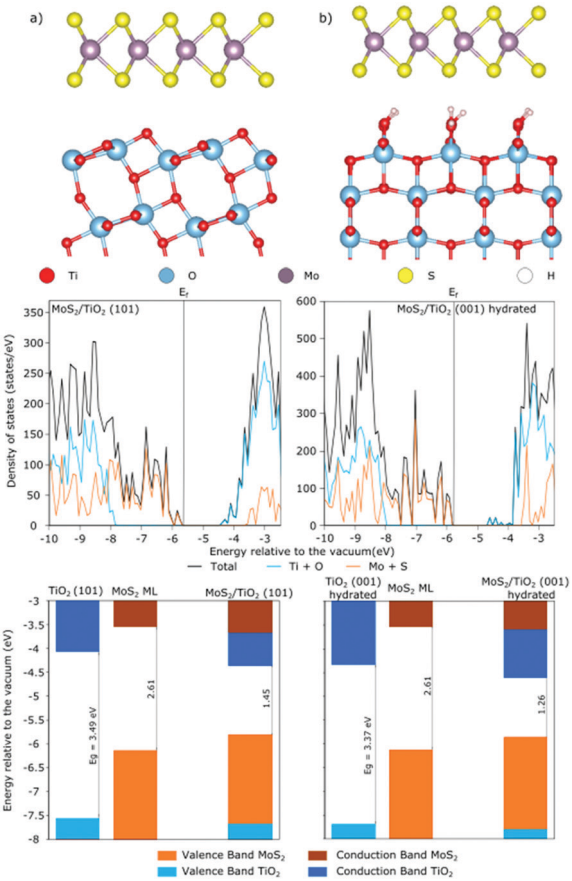

Fig. 2 Molecular structures of a MoS_2 nanosheet physically adsorbed on the two TiO_2 surfaces, DOS of these interfaces and evolution of the bands positions before and after junction for a) MoS_2/TiO_2 (101) bare and b) MoS_2/TiO_2 (001) hydrated.

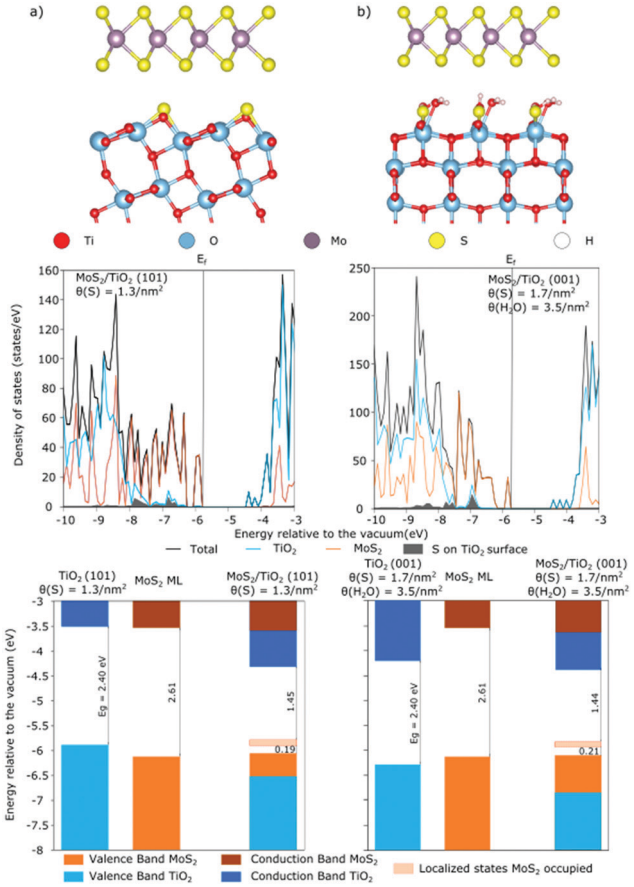

Fig. 3 Molecular structures of a MoS_2 nanosheet physically adsorbed on the two sulfided TiO_2 surfaces, DOS of the interfaces and evolution of the bands positions before and after junction for a) TiO_2 (101) with θ(S) = 1.7 S nm^{-2} (b) TiO_2 (001) with θ(S) = 1.7 S nm^{-2} and θ(H_2O) = 3.5 H_2O nm^{-2}.

localized on the Mo atoms of MoS_2 while the conduction band is localized on the Ti atoms of TiO_2. Such type of heterostructure might lead to a type II or a Z-type working principle (Fig. 1) To complete the electronic structure characterization of these interfaces, the charge transfer will be discussed later.

Sulfided and hydrated-sulfided TiO_2 surfaces. Previous DFT[42] and experimental XPS[43] studies showed that the TiO_2 surface may become sulfided under sulfiding conditions (using H_2S as sulfiding agent for instance). Hence, the substitution of surface oxygen atoms by sulfur atoms on TiO_2 is thermodynamically stabilized under such conditions. Being inspired by these former studies, we considered two sulfided TiO_2 surfaces (one for each orientation), as represented in Fig. 3 with the MoS_2 monolayer physically adsorbed on. The first one (Fig. 3a) corresponds to a substitution of two oxygen atoms by unit cell on the (101) bare surface leading to a 1.3 S nm^{-2} coverage on the surface. After optimizing the physical MoS_2/TiO_2–S heterostructure, the average distance between the two S planes (on the TiO_2 surface and on the MoS_2 nanosheet) is 2.73 Å and the average distance between the S plane of MoS_2 and the O plane of TiO_2 surface is 3.19 Å, thus larger than without sulfidation (2.87 Å), which explains the weaker adhesion energy of −0.06 eV per MoS_2.

The second one (Fig. 3b) considers the same hydration state as for the non-sulfided (001) surface and the substitution of the four oxygen atoms by sulfur atoms per unit cell, resulting in a coverage of 3.5 H_2O per nm^2 and 1.7 S nm^{-2}. After the junction with a MoS_2 the average distance between the two S planes (of the TiO_2 surface and of the MoS_2 nanosheet) is 3.42 Å (∼0.7 Å greater than in the previous case) while the average distance between the S plane of MoS_2 and the O plane of TiO_2 is now 2.86 Å smaller than before sulfidation (3.02 Å). It is explained by the fact that after optimization, 8 OH groups remain while 8 OH groups are retransformed into 4 water molecules and 4 surface oxygen, closer to the nanosheet. So, the final hydroxylation state of surface is different from the non sulfided one. The average distance between the oxygen plane of the hydroxyls and the S plane of the nanosheet is 3.12 Å (3.02 Å before sulfidation). The adhesion energy remains small (−0.10 eV per MoS_2) as in the non sulfided case, due to various compensation effects induced by van der Waals interactions and H-bonding.

The DOS with material decomposition associated to these structures (Fig. 3) shows that the 3p states of the sulfur atoms located on both sulfided TiO_2 surfaces are mainly contributing to the top of valence band of TiO_2, whereas the 2p states of oxygen were contributing on the non-sulfided surfaces. Moreover,

the 3p S states are higher in energy (~1 to 1.5 eV) with respect to the former 2p O states.

The change of the band positions after the junction, is more pronounced than for the previous non sulfided surfaces. On the sulfided (101) surface (Fig. 3a), we observe a fall of the conduction band of TiO_2 that could be driven by the sulfur–sulfur interaction across the interface. On the (001) sulfided and hydrated (Fig. 3b), this interaction is diminished due to the surface hydration. In both cases, we observe after interaction a fall of the valence band of TiO_2 (localized on the surface sulfur) and a climb of the valence band of MoS_2. The apparition of localized 4d Mo states at the top of the valence band could be induced by the shift of 3p S states of the TiO_2 surface at higher energy levels becoming closer to the top of the valence band of the MoS_2 nanosheet (than the 2p O states in the non-sulfided case).

MoS_2 nanoribbon in chemical interaction with TiO_2 anatase surfaces

Bare and hydrated TiO_2 surfaces. As discussed in Introduction, the literature reports the possibility to grow MoS_2 nanosheet on top of anatase particles by epitaxy.[31–33] In that case, we consider a nanoribbon with infinite dimension only in the direction parallel to the TiO_2 surface forming a 1D chemical interface. On the other direction, the nanoribbon implies the creation of two different edges on MoS_2 usually called "Mo-edge" and "S-edge"[44] (Fig. 4a). The more favorable restructuration (Fig. 4b) corresponding to 50% sulfur atoms (with respect to bulk reference) on each edge has been chosen for building the epitaxial structure.

The creation of these edges has a strong impact on the electronic structure associated (Fig. 5) with a strong decrease (~2 eV) of the bandgap with respect to the infinite nanosheet due to new electronic states localized on the edges. As already reported by previous DFT studies,[45] these electronic states filled the top of the valence bands and the bottom of the conduction bands.

Depending on the way the interfacial structure is prepared, its chemical composition or the size of the MoS_2 nanoribbon may change. Particularly, if the genesis of the MoS_2 nanoribbon is obtained through a sulfidation process of Mo-oxide precursor, some oxygen atoms may not be fully replaced by sulfur atoms at the interface and some Mo–O–Ti bridges may remain.[31,46] Also, the size of the MoS_2 nanoribbon can be tuned by the experimental conditions such as sulfidation temperature.[47] These chemical modifications have been tested on the finite nanoribbon (Fig. 5) but they have only a slight impact on the band positions, apart from oxygen doping which induces the apparition of a localized state and a down shift of the valence band induced by the 2p O state.

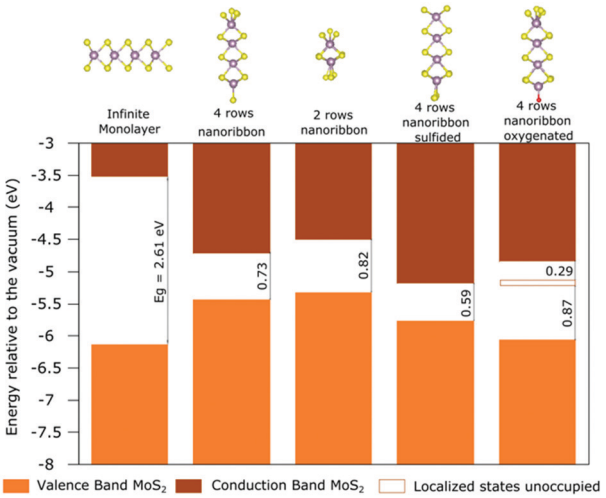

Fig. 5 Evolution of the band positions of MoS_2 from the infinite monolayer to various sizes nanoribbons and chemically modified nanoribbons.

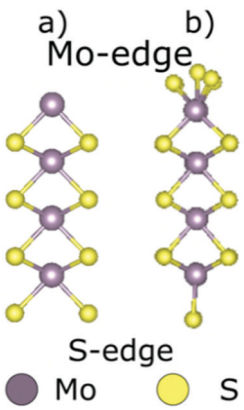

Fig. 4 Evolution of the MoS_2 finite nanoribbon before (a)) and after restructuration induced by the transfer of half of S-atoms from the S-edge to M-edge (b)).

First, we focus on the ribbon without chemical modification and we explore to which extent a chemical interaction between MoS_2 and TiO_2 surface may influence the electronic structures of the heterojunctions compared to the van der Waals heterostructures presented before. For that purpose, we consider the TiO_2 (101) bare and the TiO_2 (001) hydrated surfaces.

On the (101) surface, we optimized the interfacial systems starting from structures inspired by the one previously reported or Mo_6S_{12+x} clusters.[31,32] After optimization, the MoS_2 nanoribbon is tilted with an angle of ~40° between the Mo plane and the (101) surface. The interaction with the TiO_2 surface occurs through the so-called "Mo-edge" of MoS_2 whereas the opposite "S-edge" is free (Fig. 6a). The stabilization at interface is ensured by 4 membered ring Mo–S–Ti–O. In the case of the hydrated (001) TiO_2 surface, we revisited the possible interactions of the two MoS_2 edges: the first one through the M-edge with an angle of ~58° (Fig. 6b) and the second one through the S-edge with ~68° (Fig. 6c). The interaction is ensured through Mo–O–Ti and Mo–S–Ti bridges in the first case and Mo–S–Ti–O rings in the second one. The adhesion energies calculated using the MoS_2 nanoribbon as a reference are −0.24 eV per MoS_2 for the (101) surface, ~ 0 eV per MoS_2 for the (001) hydrated surface in interaction with the Mo-edge and −0.21 eV for the (001) hydrated surface interacting with the S-edge.

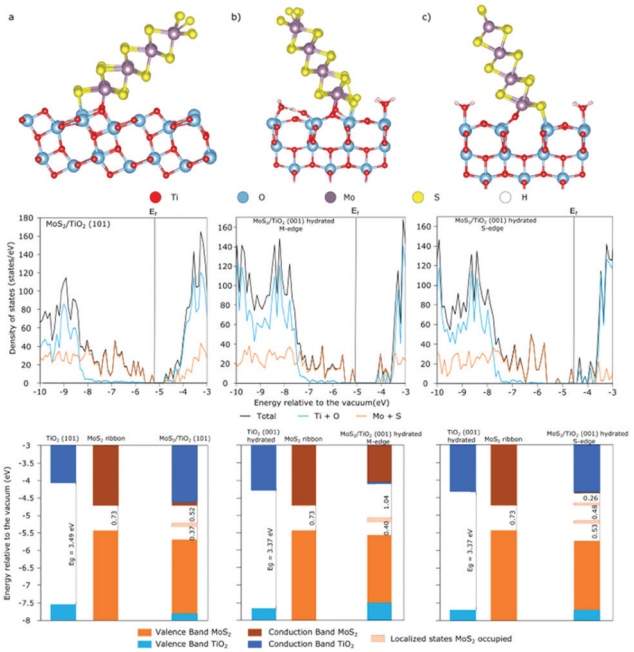

Fig. 6 Molecular structures of MoS_2 nanoribbons chemically adsorbed on the two TiO_2 surfaces, DOS of the interfaces and evolution of the bands positions before and after junction for (a) TiO_2 (101) (b) TiO_2 (001) (interaction with M-edge) and (c) TiO_2 (001) (interaction with S-edge).

The DOS associated to the systems in chemical interaction (Fig. 6) illustrates the strong impact of the chemical interaction between the two semiconductors with large differences compared to the physical interaction. Although a bandgap is maintained, several localized and occupied states, localized on MoS_2, appears in the gap. If we compare the bands positions before and after the junction (Fig. 6), the impact of the chemical bonds on the band structure is clearly visible with a large variation of the band positions. The effect on TiO_2 is visible only with the (101) surface with a small fall of the conduction band after interaction. On MoS_2, the impact is the same in all the cases, with a bandgap increased after the interaction and the apparition of these localized states. As illustrated by the spatial charge analysis (Supporting Information 7, ESI†), the occupied and unoccupied states (including localized states) close to the Fermi level are located either at the interface or at the free MoS_2 nanoribbon edge. In the case of the (101) surface (Fig. S15, ESI†) and (001) surface (Fig. S16, ESI†) in interaction with the S-edge, these localized states are at the interface whereas they are located at the free S-edge for the (001) surface in interaction with the Mo-edge (Fig. S17, ESI†). Since the CB and VB of the materials are mainly localized at the interface (the only exception is with the (001) in interaction with the S-edge), the localized states at the interface could sadly become recombination centers.

The charge transfer mechanism involves a type I heterojunction with the valence band edge and conduction band edge that could be localized on MoS_2. Since the localized states could have unwished and complicated behaviors, including the accumulation of the holes and the diminution of the global bandgap, we explored if chemical modifications of the interface or size effect of the MoS_2 nanoribbon could change the type of heterojunction and avoid the apparition of such localized states in the bandgap.

Chemical modification of the 1D-interface. We applied the same chemical modifications to the ribbon in chemical interaction with a TiO_2 surface as those applied on the nanoribbon alone (Fig. 5). Due to a significantly larger supercell of the (001) slab, these investigations have been undertaken on the (101) surface only.

The DOS associated to these structures clearly reveal the effect of these three chemical modifications on the electronic properties. The diminution of the number of Mo rows (Fig. 7a) leads to a more complex electronic structure with a smaller bandgap and still localized states at the interface (Fig. S18, ESI†) that could become recombination centers. In the cases of increased sulfidation at the free edge (Fig. 7b) or oxygenation at the interface (Fig. 7c), these localized states vanish. For the oxygenated interface, the bandgap is significantly enlarged (1.03 eV). In the sulfidation case (Fig. S19, ESI†), the CB located at the free edge and the VB which contains contribution on both edges could lead to a spatial separation of the electrons and the holes generated. The same possibility occurs for oxygenated interface (Fig. S20, ESI†), with a VB located at the interface and a CB with contribution on both edges. In the three cases, a type I heterojunction is found with the conduction and valence bands both localized on MoS_2.

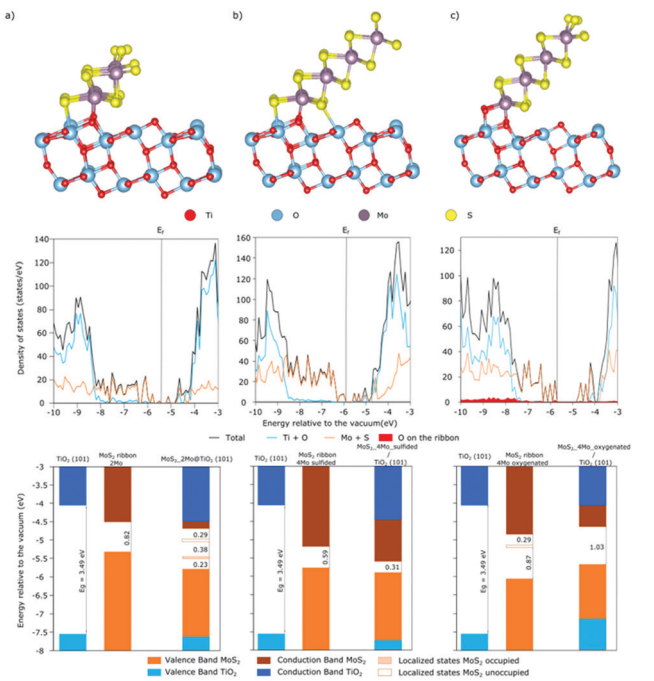

Fig. 7 Molecular structures of MoS_2 nanoribbons chemically adsorbed on the TiO_2 (101) surfaces, DOS of the interfaces and evolution of the bands positions before and after junction for (a) MoS_2 ribbon with 2 Mo rows (b) MoS_2 ribbon with 4 Mo rows sulfided and (c) MoS_2 ribbon with 4 Mo rows and oxygenated interface.

Discussion

The comparison of the band positions of all the physical interaction structures (Fig. 8) reveals that the modifications of the TiO_2 surface (such as sulfidation) induce only slight modifications in the band structures of MoS_2, because of the weak electronic interaction between the two materials. On the other hand, these modifications could modify its electronic properties. On the (001) surface, while the hydration of the surface leads to an increase of TiO_2 bandgap in comparison with the bare surface (Fig. S8, ESI†), the sulfidation of the surface induces a strong diminution of the band gap (Fig. 8), with a significant upper shift of the valence band due to the 3p states of sulfur atoms at the top of the valence band. The same trend is observed with the sulfidation of the (101) surface. All cases correspond to a type II heterojunction, and two mechanisms ("classical" or "Z-scheme", Fig. 1) could be involved depending on the dynamics of charge carriers. On the one hand, the classical type II mechanism would imply the transfer of the holes in the VB of MoS_2, and the transfer of the electrons in the CB of TiO_2. In that case, the reduction and oxidation potential are limited by the energy difference between the VB of MoS_2 and the CB of TiO_2. Alternatively, a Z-scheme mechanism would imply the recombination of the holes generated in MoS_2 with the electrons generated in TiO_2 at the interface (Fig. 9a). This induces an accumulation of electrons in MoS_2 and holes in TiO_2. In these conditions, the system will exhibit appropriate reduction and oxidation potentials, that could allow to achieve the targeted photoreduction of CO_2 on MoS_2 and oxidation of H_2O on TiO_2.

The strong effect of the sulfidation on the electronic structure (diminution of TiO_2 bandgap and apparition of a localized state), could favor one of the two mechanisms as a function of the behavior of these localized states. Depending on the mechanism, MoS_2 will act as the reducer or as the oxidizer (TiO_2 will do the opposite reaction in both cases). This could be an argument in the choice of the mechanism. To do that,

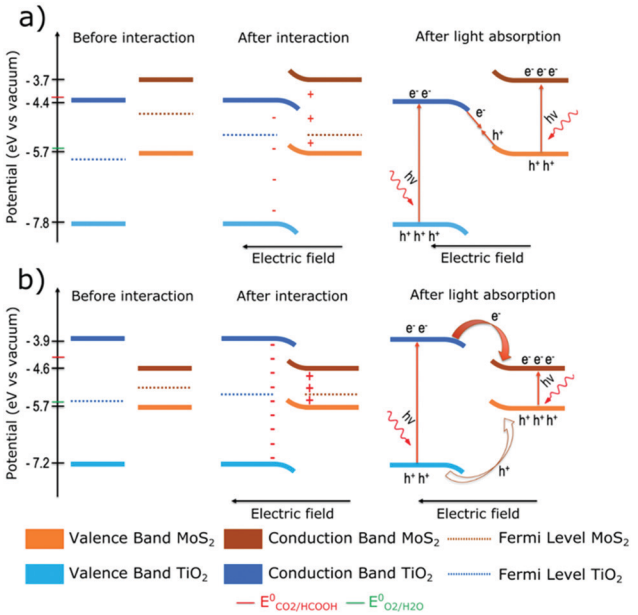

Fig. 9 (a) Possible Z-scheme mechanism for the physical 2D-heterojunction between the MoS_2 sheet and the TiO_2 (101) surface, (b) Type I heterojunction of the 1D chemical interface between MoS_2 nanoribbon (4 Mo rows oxygenated) and the TiO_2 (101) surface. Due to the intrinsic semiconductors involved, the Fermi levels are localized in the middle of the bandgap before interaction.

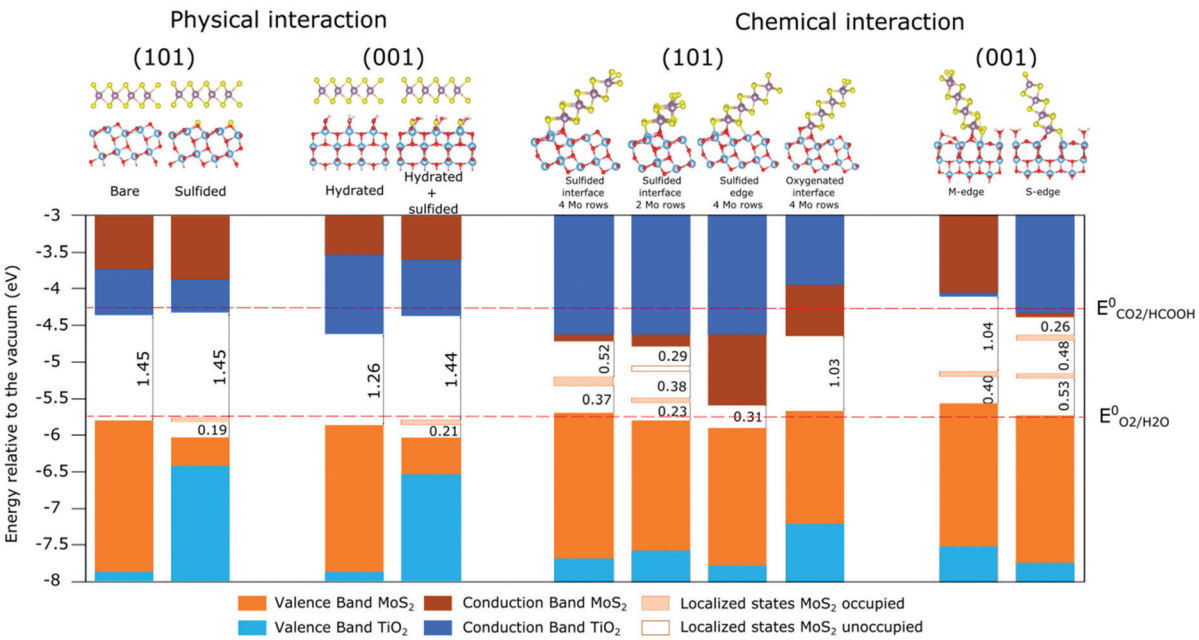

Fig. 8 Comparison of the bands positions for all heterojunctions studied in this work: in physical interaction (left panel) and chemical interaction (right panel).

tuning by sulfidation the TiO_2 surface will be needed through the modification of the pressures of H_2S and H_2O during a pre-activation step of the material.

Although a clear conclusion about the mechanism that will take place in experiment (''classical'' or ''Z-scheme'', Fig. 1) is impossible without the knowledge of dynamics of charge carriers, the distribution of charges at the interface and the resulting orientation of the internal electric field before irradiation might help to figure out if the junction will follow a classical or Z-scheme working principle Fig. 9a.[14] Hence, the calculation of the Bader charge difference[48] between the subsystems (MoS_2 nanosheet and TiO_2 surface) before and after junction has been performed (Table 1). In the case of physical interaction, a weak charge transfer occurs from one MoS_2 nanosheet to TiO_2, which is more significative with the (001) hydrated than with the (101) bare (+0.18 e^- *vs.* +0.02 e^- transferred per MoS_2 sheet). Obviously, the presence of H-bonding enhances the transfer. Reversely, for both surfaces, the transfer is significantly attenuated by sulfidation of the (001) surface or even inverted for the (101) one (+0.07 e^- and −0.04 e^-, respectively). As aforementioned, the presence of sulfur-atoms on TiO_2 surfaces induces an increase of the distance between the MoS_2 sheet and the surface. The fact that the junction involving the TiO_2 (001) hydrated surface induces such a negative charge on TiO_2 and a positive one on MoS_2 could generate the proper internal field with the expected band bending and facilitate a Z-scheme mechanism: the holes generated on MoS_2 are attracted by the negatively charged TiO_2 and the electrons generated on TiO_2 attracted by the positively charged MoS_2, which may lead to the targeted electron–hole recombination at the interface upon illumination (Fig. 9a). Moreover, the band gap of the MoS_2/(001) TiO_2 hydrated heterojunction is 0.2 eV smaller than the one of MoS_2/(101) TiO_2 which is also a parameter in favor of a Z-scheme mechanism. Hence, the formation of a heterojunction involving the hydrated (001) surface without sulfidation should be sought at the synthesis step. This result might explain in part the recent experimental studies on 2D-2D MoS_2/(001) TiO_2 nanojunctions[30] revealing a H_2 evolution rate 36.4 times higher than that of pure TiO_2. Our calculations show that the charge transfer increases thanks to a surface contact which could be explained by a Z-scheme mechanism enhancing a spatial separation of the charge carriers while maintaining a good reduction and oxidation power.

If we now summarize the band positions of the systems in chemical interaction (Fig. 8), the various MoS_2 nanoribbons lead to modifications on the electronic structure of both materials. In fact, while the modification of the number of rows and the modification of the edge leads logically to slight modifications in the band positions, the sulfur/oxygen exchange at the interface implies the modification of the interaction with the TiO_2 surface and an increase of its conduction band and valence band. Concerning MoS_2, the modification of the number of rows and the sulfidation at the edge narrow the bandgap and eliminate the localized state in the gap. It is accompanied by a shift to the lowest energy in the second case.

In the case of the oxygenated interface, the substitution of the sulfur at the interface has a low impact on MoS_2 electronic structure apart the vanishing of the localized states. Concerning the charge transfer analysis (Table 1), we observe once again an electron transfer from MoS_2 to TiO_2, except in the case with the ribbon in interaction with its S-edge. As expected, the charge transfer is stronger than with the physical interaction (higher than 0.5 electron by nanosheet in the three cases). The strongest charge transfer occurs for the MoS_2 nanoribbon of smaller size (2 Mo rows) which may be explained by the strong delocalization of charge within the nanoribbon (Fig. S18, ESI†). Reversely, the charge transfer is limited by the presence of oxygen near the surface (+0.20 for the (101) with oxygenated interface and +0.22 for the ribbon on the (001) hydrated) which is consistent with the large band gap observed for this system. The impact of the electric field induced by this charge transfer on type I heterojunction can be discussed from Fig. 9 b. Due to their respective band positions, these systems could lead to the accumulation of both electrons and holes in the conduction band and valence band of MoS_2. In this case, the material should have limited applications as heterojunctions for photocatalysis, particularly in the case of the CO_2 photoreduction. In these systems, MoS_2 should be considered mainly as a co-catalyst. Nevertheless, due to the induced electric field, the hole transfer facing a barrier could be limited. We cannot rule out the possibility that, due to this barrier, the holes remain on TiO_2 which would imply certain potential interest for photocatalytic applications due to good charge separation between TiO_2 and MoS_2: H_2O being oxidized on TiO_2 and CO_2 being reduced on MoS_2 (although the CB level might be slightly insufficient).

Table 1 Fraction of electron transferred from MoS_2 to the TiO_2 surfaces as a function of the interaction and surface types (*i.e.* a negative value indicates a loss of electron from MoS_2)[48]

Interaction type	Interfacial structure	Δe^- MoS_2 (per nanosheet)	Δe^- TiO_2
2D-Physical	(101) bare - infinite sheet	−0.02	+0.04
	(101) sulfided - infinite sheet	+0.04	−0.09
	(001) hydrated - infinite sheet	−0.18	+0.36
	(001) hydrated and sulfided - infinite sheet	−0.07	+0.15
1D-Chemical	(101) - Mo-edge (ribbon with 4 Mo rows)	−0.52	+1.04
	(101) - Mo-edge (2 Mo rows)	−0.62	+1.25
	(101) - Mo-edge sulfided free edge (4 Mo rows)	−0.51	+1.02
	(001) - oxygenated interface (4 Mo rows)	−0.19	+0.39
	(001) - Mo-edge (4 Mo rows)	−0.22	+0.44
	(001) - S-edge (4 Mo rows)	+0.14	−0.28

Conclusions

Thanks to state of the art DFT calculations including the HSE06 functional, we showed how the various possible structural modifications of the MoS_2/TiO_2 heterojunction impact the resulting electronic properties: band gaps and CB/VB band positions. In particular, we distinguished the effects of a physical interaction and a chemical one between the MoS_2 and TiO_2 materials on the nature of the MoS_2/TiO_2 heterojunctions. A physical 2D-interface may lead to a type II or Z-scheme formalism. The analysis of the CBE/VBE band positions revealed that the physical interaction is compatible with a photocatalytic reduction process of CO_2. Moreover, a weak but non-negligible charge transfer occurs from the MoS_2 nanosheet to the hydroxylated (001) surface of TiO_2 which may induce of a Z-scheme mechanism more efficient for photon absorption processes in photocatalysis applications with reduction of CO_2 on MoS_2 and oxidation of H_2O on TiO_2. The sulfidation of the TiO_2 surface does not improve the resulting electronic properties. By contrast, all chemical 1D-interfacial systems between MoS_2 nanoribbons and TiO_2 surfaces imply the formation of a type I heterojunction. The chemical interaction induces a stronger charge transfer at the interface than for the physical interaction but the type I mode will not obligatory enhance the photon absorption efficiency during photocatalysis, except if the barrier for the hole transfer is too high and constrains the hole on TiO_2 while electrons are transferred to MoS_2.

We hope that our theoretical work quantifying the sensitivity of the electronic properties with respect to atomic scale modifications of the MoS_2/TiO_2 heterostructure will help to provide more rational guides to tune such heterojunction. A perspective of this work would be to evaluate the efficiency of these interfaces to perform the photocatalytic CO_2 reduction either by using the Computational Hydrogen Electrode[49,50] or even using the Grand Canonical DFT.[51]

Author contributions

P. R. and T. L. B. designed the research plan. R. F. conducted the DFT calculations and drafted the manuscript. P. R. and T. L. B. supervised the thesis research. All authors participated data analysis and manuscript writing.

Conflicts of interest

There are no conflicts to declare.

Acknowledgements

This work is part of the ''RatiOnAl Design for CATalysis'' (ROAD4CAT) industrial chair, project IDEXLYON funded by the French National Research Agency (ANR-16-IDEX-0005) and the Commissariat-General for Investment (CGI) within the framework of Investissements d'Avenir program (''Investment for the future''). The authors thank the SYSPROD project and AXELERA Pôle de Compétitivité for financial support (PSMN Data Center). This work was granted access to the HPC resources of CINES, IDRIS and TGCC under the allocation 2018-080609 made by GENCI.

References

1 A. Kudo and Y. Miseki, *Chem. Soc. Rev.*, 2009, **38**, 253–278.
2 M. G. Walter, E. L. Warren, J. R. McKone, S. W. Boettcher, Q. Mi, E. A. Santori and N. S. Lewis, *Chem. Rev.*, 2010, **110**, 6446–6473.
3 X. C. Chen, S. Shen, L. Guo and S. S. Mao, *Chem. Rev.*, 2010, **110**, 6503–6570.
4 W. Tu, Y. Zhou and Z. Zou, *Adv. Mater.*, 2014, **26**, 4607–4626.
5 X. Chang, T. Wang and J. Gong, *Energy Environ. Sci.*, 2016, **9**, 2177.
6 U. Kang, D. S. Han, S. K. Choi, D. J. Ham, S. M. Ji, W. Choi, D. S. Han, A. Abdel-Wahab and H. Park, *Energy Environ. Sci.*, 2015, **8**, 2638.
7 U. Ulmer, T. Dingle, P. N. Duchesne, R. H. Morris, A. Tavasoli, T. Wood and G. A. Ozin, *Nat. Commun.*, 2019, 1–12.
8 A. B. Laursen, S. Kegnaes, S. D. Dahl and I. Chorkendorff, *Energy Environ. Sci.*, 2012, **5**, 5577.
9 L. Qian, Z. Ning, Y. Yong, W. Guozhong and H. L. N. Dickon, *Langmuir*, 2014, **30**, 8965–8972.
10 M. Shahrokhi, P. Raybaud and T. Le Bahers, *ACS Appl. Mater. Interfaces*, 2021, **13**, 36465–36474.
11 A. R. Beal and H. P. Hughes, *J. Phys. C: Solid State Phys.*, 1979, **12**, 881–890.
12 K. F. Mak, C. Lee, J. Hone, J. Shan and T. F. Heinz, *Phys. Rev. Lett.*, 2010, **105**, 136805.
13 P. Zhou, J. Yu and M. Jaroniec, *Adv. Mater.*, 2014, **26**, 4920–4935.
14 X. Li, C. Garlisi, Q. Guan, S. Anwer, K. Al-Ali, G. Palmisano and L. Zheng, *Mater. Today*, 2021, **47**, 75–107.
15 B. Chen, Y. Meng, J. Sha, C. Zhong, W. Hu and N. Zhao, *Nanoscale*, 2018, **10**, 34–68.
16 C. Maheu, E. Puzenat, C. Geantet, L. Cardenas and P. Afanasiev, *Int. J. Hydrogen Energy*, 2019, **44**, 18038–18049.
17 A. Fujishima, X. Zhanj and D. A. Tryk, *Surf. Sci. Rep.*, 2008, **63**, 515–582.
18 A. L. Linsebigler, G. Lu and J. T. Yates Jr, *Chem. Rev.*, 1995, **95**, 735–758.
19 C. G. Morales-Guio, L.-A. Stern and X. Hu, *Chem. Soc. Rev.*, 2014, **43**, 6555–6569.
20 R. Arancon, M. Saab, A. Morvan, A. Bonduelle-Skrzypczak, A.-L. Taleb, A.-S. Gay, C. Legens, O. Ersen, K. Searles, V. Mougel, A. Fedorov, C. Copéret and P. Raybaud, *J. Phys. Chem. C*, 2019, **123**, 24659–24669.
21 W. Zhang, X. Xiao, Y. Li, X. Zheng, L. Zheng and C. Whan, *RSC Adv.*, 2016, **6**, 33705–33712.
22 X. Liu, Z. Xing, H. Zhang, W. Wang, Y. Zhang, Z. Li, X. Wu, X. Yu and W. Zhou, *ChemSusChem*, 2016, **9**, 1118–1124.
23 W. Tu, Y. Li, L. Kuai, Y. Zhou, Q. Xu, H. Li, X. Wang, M. Xiao and Z. Zou, *Nanoscale*, 2017, **9**, 9065–9070.

24 S. Kanda, T. Akita, M. Fujishima and H. Tada, *J. Colloid Interface Sci.*, 2011, **354**, 607–610.
25 M. Shen, Z. Yan, L. Yang, P. Du, J. Zhang and B. Xiang, *Chem. Commun.*, 2014, **50**, 15447–15449.
26 W. Zhou, Z. Yin, Y. Du, X. Huang, Z. Zeng, Z. Fan, H. Liu, J. Wang and H. Zhang, *Small*, 2013, **9**, 140–147.
27 X. Zhou, M. Lickleder and P. Schmuki, *Electrochem. Commun.*, 2016, **73**, 33–37.
28 M. Lazzeri, A. Vittadini and A. Selloni, *Phys. Rev. B: Condens. Matter Mater. Phys.*, 2001, **63**, 155409.
29 C. Arrouvel, M. Digne, M. Breysse, H. Toulhoat and P. Raybaud, *J. Catal.*, 2004, **222**, 152–166.
30 Y.-J. Yuan, Z.-J. Ye, H. Lu, B. Hu, Y.-H. Li, D. Chen, J.-S. Zhong, Z.-T. Yu and Z. Zou, *ACS Catal.*, 2016, **6**, 532–541.
31 C. Arrouvel, M. Breysse, H. Toulhoat and P. Raybaud, *J. Catal.*, 2005, **232**, 161–178.
32 D. Costa, C. Arrouvel, M. Breysse, H. Toulhoat and P. Raybaud, *J. Catal.*, 2007, **246**, 325–343.
33 Y. Sakashita, Y. Araki, K. Honna and H. Shimada, *Appl. Catal., A*, 2000, **197**, 247–253.
34 G. Kresse and J. Furthmüller, *Comput. Mater. Sci.*, 1996, **6**, 15–50.
35 G. Kresse and J. Furthmüller, *Phys. Rev. B: Condens. Matter Mater. Phys.*, 1996, **54**, 11169–11186.
36 J. P. Perdew, K. Burke and M. Ernzerhof, *Phys. Rev. Lett.*, 1996, **77**, 3865–3868.
37 J. Heyd and G. E. Scuseria, *J. Chem. Phys.*, 2004, **121**, 1187–1192.
38 S. Grimme, S. Ehrlich and L. Goerigk, *J. Comput. Chem.*, 2011, **32**, 1456–1465.
39 K. Mattew, R. Sundararaman, K. Letchworth-Weaver, T. A. Arias and R. G. Hennig, *J. Chem. Phys.*, 2014, **140**, 084106.
40 J. Kullgren, B. Aradi, T. Frauenheim, L. Kavan and P. Deak, *J. Phys. Chem. C*, 2015, **119**, 21952–21958.
41 H. Han, K. M. Kim, C.-W. Lee, C. S. Lee, R. C. Pawar, J. L. Jones, Y.-R. Hong, J. H. Ryu, T. Song, S. H. Kang, H. Choi and S. Mhin, *Phys. Chem. Chem. Phys.*, 2017, **19**, 28207–28215.
42 C. Arrouvel, H. Toulhoat, M. Breysse and P. Raybaud, *J. Catal.*, 2004, **226**, 260–272.
43 L. Coulier, J. van Veen and J. Niemantsverdriet, *Catal. Lett.*, 2002, **79**, 149–155.
44 H. Schweiger, P. Raybaud, G. Kresse and H. Toulhoat, *J. Catal.*, 2002, **207**, 76–87.
45 P. Raybaud, J. Hafner, G. Kresse, S. Kasztelan and H. Toulhoat, *J. Catal.*, 2000, **189**, 129–146.
46 R. G. Leliveld, A. J. van Dillen, J. W. Geus and D. C. Koningsberger, *J. Catal.*, 1997, **165**, 184–196.
47 B. Baubet, A.-S. Gay, A.-L. Taleb, M. Moreaud, F. Wahl, V. Delattre, E. Devers, A. Hugon, O. Ersen, P. Afanasiev and P. Raybaud, *ACS Catal.*, 2016, **6**, 1081–1092.
48 R. F. W. Bader, *Atoms in Molecules – A Quantum Theory*, Oxford university press, New York, 1990.
49 M. Bajdich, M. Garcia-Mota, A. Vojvodic, J. K. Nørskov and A. T. Bell, *J. Am. Chem. Soc.*, 2013, **135**, 13521–13530.
50 L. Lv, Y. Shen, X. Gao, J. Liu, S. Wu, Y. Ma, X. Wang, D. Gong and Z. Zhou, *Appl. Surf. Sci.*, 2021, **546**, 149066.
51 A. Curutchet, P. Colinet, C. Michel, S. N. Steinmann and T. Le Bahers, *Phys. Chem. Chem. Phys.*, 2020, **22**, 7031–7038.